

In-medium polarization tensor in strong magnetic fields (II): Axial Ward identity at finite temperature and density

Koichi Hattori^{1,2} and Kazunori Itakura^{3,4}

¹*Zhejiang Institute of Modern Physics, Department of Physics,
Zhejiang University, Hangzhou, 310027, China*

²*Research Center for Nuclear Physics,
Osaka University, Osaka 567-0047 Japan.*

³*Nagasaki Institute of Applied Science (NiAS),
536 Aba-machi, Nagasaki-shi, Nagasaki, 851-0193, JAPAN*

⁴*High-Energy Accelerator Research Organization (KEK),
1-1 Oho, Tsukuba, Ibaraki, 305-0801, JAPAN*

Abstract

We investigate the axial Ward identity (AWI) for massive fermions in strong magnetic fields. The divergence of the axial-vector current is computed at finite temperature and/or density with the help of a relation between the polarization and anomaly diagrams in the effective (1+1) dimensions realized in the lowest Landau level (LLL). We discuss delicate interplay between the vacuum and medium contributions that determines patterns of the spectral flow in the adiabatic limit and, more generally, the diabatic chirality production rate. We also establish an explicit relation between the AWIs from the LLL approximation and from the familiar triangle diagrams in the naive perturbative series with respect to the coupling constant.

CONTENTS

I. Introduction	2
II. Vector and axial Ward identities	6
III. Polarization tensor	7
IV. Axial Ward identity in strong magnetic fields	10
A. Summary of the results	10
B. Vacuum contributions	13
1. Massless case	13
2. Massive case	14
C. Medium contributions	17
1. Spectral flow in medium	17
2. Diabatic processes	19
V. Summary and discussions	22
A. Massless fermions and antifermions in the LLL	24
B. Chiral anomaly diagram with massive LLL fermions	26
C. Relation to the triangle diagrams	28
References	31

I. INTRODUCTION

In this series of papers, we investigate the polarization effects of the medium particles at finite temperature and/or density as well as of the vacuum fluctuations in strong magnetic fields. In the first paper [1], which is referred to as Paper I, we have provided the explicit forms of the vacuum and medium contributions to the one-loop polarization tensor in the lowest Landau level (LLL) approximation and discussed magneto-birefringence as a physical application, that is, the polarization-dependent photon dispersion relation induced by

the strong magnetic fields. We have inspected delicate interplay between the vacuum and medium contributions.

In the second paper of the series, we discuss another application of the polarization tensor to the axial-charge generation. Although the polarization tensor is a current correlator of the vector-vector type, one can apply it to the induction of the axial-vector current because there is an identity between the vector and axial-vector currents expanded with the eigenstates of the Landau levels. This identity is an analogue of that in the (1+1)-dimensional QED and the physical reason behind this identity is the chirality-momentum locking in the spin eigenstates (see Sec. II for more details).

Mechanisms of the axial-charge generation have attracted much attention over the last decade since a nonzero axial charge implies a parity-odd environment and induces transport phenomena that do not occur in parity-even environments. One of the prominent examples is induction of an electric current in magnetic fields, which is known as the chiral magnetic effect (CME) [2, 3]. The anomalous transport phenomena have been intensively investigated in the contexts of quark-gluon plasma created by relativistic heavy-ion collisions [4–6] and of the Weyl and Dirac semimetals in condensed matter physics [7–9]. The chiral magnetic effect, together with Ampère’s law, further implies an exponential growth of the magnetic-field strength driven by a positive feedback cycle when the magnetic field is lifted to a dynamical field. This is called the chiral plasma instability [10] and is expected to be possible mechanisms for generation of the strong magnetic fields during supernova explosions [11, 12] and of the primordial magnetic field in the early universe [13–18]. Those hot situations, including the very recent CME search by isobaric collisions [19], motivate us to investigate the axial-charge generation. Although the CME conductivity is given by a universal form stemming from chiral anomaly, it is also proportional to the magnitude of the axial chemical potential that is a thermodynamic conjugate quantity to the axial-charge density and depends on dynamics in individual systems. To name a few, the axial-charge dynamics was investigated in Refs. [20–27] for relativistic heavy-ion collisions, Refs. [28, 29] for neutron-star physics, and Refs. [30, 31] for cosmology.

We investigate the axial-charge generation from a fundamental point of view in terms of the divergence of the axial-vector current. QED contains chiral anomaly [32, 33], giving rise to the anomalous nonvanishing term in the divergence of the axial-vector current. A finite fermion mass explicitly breaks the chiral symmetry, and gives rise to another nonvanishing

term in the divergence of the current. In case of (3+1)-dimensional QED, the well-known triangle diagrams yield both of those two nonvanishing contributions when the loop diagrams are composed of massive fermions.

There is, however, a significant difference between those two pieces of the same diagrams. The anomalous term does not receive radiative corrections [34]; The anomalous term stems from the (superficial) ultraviolet divergence of the triangle diagrams, so that, without modifications of the divergent pole, there is no correction to the anomalous term. This means that there is no correction from the fermion mass or other external parameters such as temperature or density that do not modify the divergent pole [35]. In contrast, the mass-dependent part does not involve an ultraviolet divergence and can come with temperature and/or density corrections. The whole non-conservation equation of the axial-vector current, which we call the axial Ward identity (AWI), is controlled by the balance between the anomalous and mass-dependent terms that arise from the divergent and finite pieces of the loop integral.¹

Since the mass-dependent part in the AWI is not anomalous in nature, it does not exhibit simple behaviors in general when one varies magnitudes of relevant parameters such as the external photon momenta, fermion mass, temperature and/or density. Therefore, the AWI as a whole is not simply governed by the anomalous term and, moreover, the two terms can be comparable in magnitude, implying that the axial-vector current could be effectively conserved in some parameter regimes. Thus, we investigate the whole AWI with explicit computations.

Relevant processes for the axial-charge generation can be classified into *adiabatic* and *diabatic* processes according to the magnitude of energy transfer from the external photon fields (see Sec. IV A for a more precise definition). The adiabatic processes can be understood as the spectral flow that is a collective flow of the occupied states along the fermion dispersion relation [36, 37] (see also Ref. [38] for a review). The adiabatic flows occur when there is no energy transfer from the photon fields to the fermions and are only the processes for which one can get simple results. One should notice that the spectral flow occurs on the thermally occupied positive-energy states as well as on the negative-energy states beneath the Dirac sea, and induces the helicity flip at the bottom of the parabolic dispersion relation for massive fermions. In the other cases, i.e., the diabatic processes, nonzero energy transfer

¹ The mass-dependent part may not be saturated with the finite piece of the anomaly diagrams, and could be subject to higher-order or any kind of corrections due to the non-divergent nature.

can induce intricate excitations that ruin the ordered collective flows. Such information is all encoded in the mass-dependent part. We provide a more detailed summary of the results in Sec. IV A.

Incidentally, we also explicitly show a connection between the AWIs from the triangle diagrams and from the polarization tensor in the LLL approximation. Chiral anomaly is often explained as a product of the (1+1)-dimensional chiral anomaly and the Landau degeneracy factor on the basis of the effective dimensional reduction in the LLL [36]. The explicit computation of the LLL contribution, however, does not exactly reproduce the result from the triangle diagrams due to an extra Gaussian factor that stems from the fermion wave function in the LLL. This is simply because the wave function of the LLL fermion is not exactly (1+1) dimensional one, but has an extension in perpendicular to the magnetic field. The Gaussian factor reduces to unity in the homogeneous electric-field limit and/or the strong magnetic field limit such that the electric field does not resolve the transverse extension of the cyclotron orbits. As for the mass-dependent part, the LLL approximation reproduces that from the triangle diagrams when the *constant* magnetic field limit is taken for the triangle diagrams, again up to the Gaussian factor.

This paper is organized as follows. In Sec. II, we provide basic formulas for the induction of the vector and axial-vector currents by a single two-point correlator in the LLL approximation. In Sec. III, we summarize the explicit expressions of the polarization tensor from Paper I for readers' convenience. Then, we discuss the AWI in detail in Sec. IV. In appendices, we clarify the quantum numbers characterizing the fermions in the LLL and perform an explicit computation of the divergence of the axial current composed of a massive Dirac fermion in the LLL, reproducing the expression from the polarization tensor. Finally, we discuss a connection between the AWIs computed from the LLL approximation and the triangle diagrams in Appendix C.

As in Paper I, we focus on a single-flavor Dirac fermion with an electric charge q_f for simplicity, and introduce a single chemical potential conjugate to its number density. We also assume that a constant magnetic field is applied along the third spatial direction without losing generality, i.e., $\mathbf{B} = (0, 0, B)$. Accordingly, we use metric conventions $g^{\mu\nu} = \text{diag}(1, -1, -1, -1)$, $g_{\parallel}^{\mu\nu} = \text{diag}(1, 0, 0, -1)$, and $g_{\perp}^{\mu\nu} = (0, -1, -1, 0)$ and associated notations $q_{\parallel}^2 := q_{\mu}q_{\nu}g_{\parallel}^{\mu\nu}$ and $q_{\perp}^2 := q_{\mu}q_{\nu}g_{\perp}^{\mu\nu} = -|\mathbf{q}_{\perp}|^2$ for four vectors q^{μ} .

II. VECTOR AND AXIAL WARD IDENTITIES

The retarded polarization tensor serves as a linear response function with respect to electromagnetic perturbations. In this paper, we discuss induction of the currents transported by the LLL fermions

$$j_V^\mu = q_f \bar{\psi}_{\text{LLL}} \gamma^\mu \psi_{\text{LLL}}, \quad (1a)$$

$$j_A^\mu = \bar{\psi}_{\text{LLL}} \gamma^\mu \gamma^5 \psi_{\text{LLL}}. \quad (1b)$$

The fermion spinor ψ_{LLL} in the LLL is an eigenstate of the spin projection operator $\mathcal{P}_+ = (1 + i s_f \gamma^1 \gamma^2)/2$ with the sign function $s_f = \text{sgn}(q_f B)$. By the use of an identity among the gamma matrices $\gamma_\parallel^\mu \gamma^5 \mathcal{P}_\pm = \mp s_f \epsilon_\parallel^{\mu\nu} \gamma_\nu \mathcal{P}_\pm$, we find a relation between the LLL contributions to the vector and axial-vector currents along the magnetic field²

$$q_f j_A^\mu = -s_f \epsilon_\parallel^{\mu\nu} j_{V\nu}, \quad (2)$$

where we introduced an antisymmetric tensor $\epsilon_\parallel^{\mu\nu}$ which only has two non-vanishing components, $\epsilon_\parallel^{03} = -\epsilon_\parallel^{30} = 1$. This relation is an analogue of the well-known relation in the (1+1) dimensional QED (see, e.g., a standard textbook [39]) and is understood as a consequence of the effective dimensional reduction. Equation (2) relates the vector–vector (VV) correlator $\Pi_R^{\mu\nu}$, that we inspected in Paper I, to the vector–axial-vector (VA) correlator

$$\langle j_A^\mu j_V^\nu \rangle_R = -s_f \epsilon_\parallel^\mu{}_\rho q_f^{-1} \Pi_R^{\rho\nu}. \quad (3)$$

The above vector and axial-vector currents are induced in response to an external $U(1)$ gauge field A^μ . This is an external gauge field with an arbitrary frequency and wavelength, superimposed on top of the constant magnetic field. When the polarization tensor has a gauge-invariant tensor structure [see Eq. (5)], the vector and axial Ward identities read

$$\text{F.T. } \partial_\mu j_V^\mu = -i q_\mu \Pi_R^{\mu\nu} A_\nu = 0, \quad (4a)$$

$$\text{F.T. } \partial_\mu j_A^\mu = -i q_\mu \langle j_A^\mu j_V^\nu \rangle_R A_\nu = s_f q_f^{-1} \Pi_\parallel \tilde{E}_\parallel(q), \quad (4b)$$

where F.T. stands for the Fourier transform and $\tilde{E}_\parallel(q) = -i \epsilon_\parallel^{\mu\nu} q_\mu A_\nu$ is the parallel (or antiparallel) component of an electric field along the magnetic field. We put tilde on the

² Here, an electric charge is not included in the definition of the axial-vector current (1b), while it is included in the vector current (1a) and the electromagnetic coupling $j_V^\mu A_\mu$ in Eq. (4b).

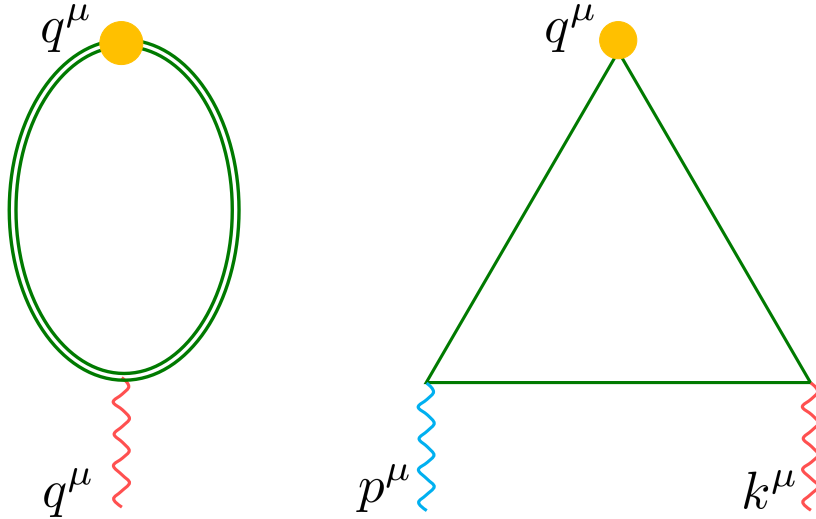


FIG. 1. One-loop polarization tensor in strong magnetic fields [left] and the triangle diagram (with an exchange diagram not shown) [right]. The double lines show the fermion propagators in the LLL approximation that have insertions of the magnetic-field lines (not shown).

electric field to emphasize that it is the Fourier spectrum, while the magnetic field B (and \mathbf{B} appearing below) is the constant magnitude throughout this paper. The vector Ward identity (4a) is a consequence of the gauge invariance in QED. However, the axial current is not conserved if the right-hand side in Eq. (4b) is nonzero. The magnitude of the nonvanishing divergence is controlled by the scalar function Π_{\parallel} from the polarization tensor. In the next section, we provide the explicit form of Π_{\parallel} from the vacuum and medium contributions.

III. POLARIZATION TENSOR

In Paper I, we provided detailed accounts on the computation of the polarization tensor in the LLL approximation (cf. the left panel in Fig. 1). Here, we briefly summarize its explicit form for readers' convenience.

In the LLL approximation, one obtains the polarization tensor

$$\Pi^{\mu\nu} = m_B^2 e^{-\frac{|q_{\perp}|^2}{2|q_{\parallel} B|}} \tilde{\Pi}_{\parallel} \mathcal{P}_{\parallel}^{\mu\nu}, \quad (5)$$

where $m_B^2 = |q_f B|/(2\pi) \cdot q_f^2/\pi$. The gauge-invariant tensor structure is given as

$$\mathcal{P}_{\parallel}^{\mu\nu} = g_{\parallel}^{\mu\nu} - \frac{q_{\parallel}^{\mu} q_{\parallel}^{\nu}}{q_{\parallel}^2}, \quad (6)$$

with the photon momentum q^{μ} . Note that this tensor structure cannot be split into the longitudinal and transverse components with respect to the spatial photon momentum, because of its dimensionally reduced form. Therefore, this is the unique gauge-invariant tensor structure within the LLL approximation. There are some other tensor structures when the higher Landau levels contribute (see, e.g., Refs. [40, 41]). The polarization function $\tilde{\Pi}_{\parallel}$ contains both the vacuum and medium contributions

$$\tilde{\Pi}_{\parallel} = \tilde{\Pi}_{\parallel}^{\text{vac}}(q_{\parallel}^2) + \tilde{\Pi}_{\parallel}^{\text{med}}(\omega, q_z). \quad (7)$$

The medium contribution $\tilde{\Pi}_{\parallel}^{\text{med}}(\omega, q_z)$ depends on the photon energy ω and momentum q_z separately, because the presence of medium breaks the Lorentz-boost invariance. Note also that we apply a constant magnetic field \mathbf{B} in the medium rest frame. Configurations composed of constant magnetic fields in other Lorentz frames are not equivalent to the present configuration.

The explicit diagram computation provides the vacuum contribution (see the appendix in Paper I)

$$\tilde{\Pi}_{\parallel}^{\text{vac}}(q_{\parallel}^2) = 1 - I\left(\frac{q_{\parallel}^2}{4m^2}\right). \quad (8)$$

Since the overall factor of m_B^2 is a dimension-two quantity in Eq. (5), the I function can only be a function of a dimensionless variable:

$$I(x + i\omega\epsilon) = \begin{cases} \frac{1}{2} \frac{1}{\sqrt{x(x-1)}} \ln \frac{\sqrt{x(x-1)}-x}{\sqrt{x(x-1)}+x} & x < 0 \\ \frac{1}{\sqrt{x(1-x)}} \arctan \frac{x}{\sqrt{x(1-x)}} & 0 \leq x < 1 \\ \frac{1}{2} \frac{1}{\sqrt{x(x-1)}} \left[\ln \frac{x-\sqrt{x(x-1)}}{x+\sqrt{x(x-1)}} + i \operatorname{sgn}(\omega)\pi \right] & 1 \leq x \end{cases}. \quad (9)$$

We took the retarded prescription $\omega \rightarrow \omega + i\epsilon$ that yields an infinitesimal displacement $q_{\parallel}^2 \rightarrow q_{\parallel}^2 + i\omega\epsilon$. The advanced and causal correlators can be computed in the same manner. One can find two limiting behaviors

$$I(0) = 1, \quad I(\infty) = 0. \quad (10)$$

Therefore, in the infinite-mass limit $q_{\parallel}^2/m^2 \rightarrow 0$, we simply find that $\tilde{\Pi}_{\parallel}^{\text{vac}} \rightarrow 0$ because the fermion excitations are suppressed. In the massless limit $q_{\parallel}^2/m^2 \rightarrow \infty$, we have

$$\tilde{\Pi}_{\parallel}^{\text{vac}}(q_{\parallel}^2) = 1. \quad (11)$$

The factor of $|q_f B|/(2\pi)$ in m_B^2 is called the Landau degeneracy factor. The remaining factor q_f^2/π is known as the Schwinger mass in the (1+1) dimensional massless QED [42, 43] that provides a photon mass in the gauge-invariant way.

The medium contribution is obtained as (see Ref. [44] and Paper I)

$$\tilde{\Pi}_{\parallel}^{\text{med}}(\omega, q_z) = \pi m^2 \int_{-\infty}^{\infty} \frac{dp_z}{2\pi\epsilon_p} \frac{(q_{\parallel}^2 + 2q_z p_z) [n_+(\epsilon_p) + n_-(\epsilon_p)]}{q_{\parallel}^2 (p_z - \frac{1}{2}q_z)^2 - \frac{\omega^2}{4}(q_{\parallel}^2 - 4m^2)}, \quad (12)$$

where the fermion energy and distribution function are given as $\epsilon_p = \sqrt{p_z^2 + m^2}$ and $n_{\pm}(\epsilon_p) = [e^{(\epsilon_p \mp \mu)/T} + 1]^{-1}$, respectively. Notice that the medium contribution is proportional to the fermion mass and does not exist in the strictly massless case. The integrand has two poles at

$$p_z^{\pm} := \frac{1}{2} \left(q_z \pm \omega \sqrt{1 - 4m^2/q_{\parallel}^2} \right). \quad (13)$$

Thus, the integrand in Eq. (12) can be rearranged as

$$\tilde{\Pi}_{\parallel}^{\text{med}}(\omega, q_z) = \frac{2\pi m^2}{q_{\parallel}^2 \sqrt{1 - 4m^2/q_{\parallel}^2}} \int_{-\infty}^{\infty} \frac{dp_z}{2\pi\epsilon_p} [n_+(\epsilon_p) + n_-(\epsilon_p)] \left(\frac{\epsilon_p^+ s_+}{p_z - p_z^+} - \frac{\epsilon_p^- s_-}{p_z - p_z^-} \right), \quad (14)$$

where we defined

$$s_{\pm} = \text{sgn} \left(\omega \pm q_z \sqrt{1 - 4m^2/q_{\parallel}^2} \right) = \text{sgn}(\omega) \theta(q_{\parallel}^2 - 4m^2) \pm \theta(-q_{\parallel}^2), \quad (15a)$$

$$\epsilon_p^{\pm} = \sqrt{(p_z^{\pm})^2 + m^2} = \frac{1}{2} \left| \omega \pm q_z \sqrt{1 - 4m^2/q_{\parallel}^2} \right|, \quad (15b)$$

for $1 - 4m^2/q_{\parallel}^2 \geq 0$ and

$$s_{\pm} = 1, \quad (16a)$$

$$\epsilon_p^{\pm} = \frac{1}{2} \left(\omega \pm i q_z \sqrt{|1 - 4m^2/q_{\parallel}^2|} \right), \quad (16b)$$

for $1 - 4m^2/q_{\parallel}^2 < 0$.

Lastly, we give some comments on the imaginary part of the polarization tensor. The imaginary part in Eq. (9) indicates occurrence of a fermion-antifermion pair creation when the photon momentum satisfies the threshold condition $q_{\parallel}^2 \geq (2m)^2$ that is the invariant

mass of a pair in the LLL states (cf. Paper I). In the massless limit (11), an imaginary part only comes from the q_{\parallel}^2 pole in Eq. (6).³ The imaginary part is thus proportional to $\delta(q_{\parallel}^2)$, meaning that there is no invariant energy transfer from a photon to a fermion-antifermion pair. Such a pair creation does not usually happen in (3+1) dimensions since a hole state in the Dirac sea needs to be created by a *diabatic* transition of a particle from the negative- to positive-energy branches. The pair creation in an *adiabatic* process can occur only because the positive- and negative-energy states are directly connected with each other in the (1+1)-dimensional gapless dispersion relation. Namely, the massless pair creation here can be interpreted as the spectral flow along the linear dispersion relation that occurs independently in the right- and left-handed sectors, leading to chiral anomaly. There is no medium correction in the massless case. The medium contribution (14) acquires imaginary parts in the massive case when the fermion and antifermion pair takes the energy ϵ_p^{\pm} and momentum p_z^{\pm} as we inspected in Paper I. The created massive pairs possess nonzero axial charges.

IV. AXIAL WARD IDENTITY IN STRONG MAGNETIC FIELDS

A. Summary of the results

In the following, we find that the AWI (4b) takes various forms depending on the scalar function Π_{\parallel} stemming from the polarization tensor. Such behaviors crucially depend on whether fermions are massive or massless and whether there is the medium contribution or not. We provide summary of the characteristic behaviors before going into detailed discussions. The reasons/interpretations leading to those results are given in the following subsections.

In the strictly massless case, it is well-known that the divergence of the axial current is saturated by the anomalous term proportional to the pseudoscalar inner product of the electromagnetic field. It is thus useful to take this case as a reference result to other limits. Inserting the polarization tensor (11) into Eq. (4b), one finds the AWI

$$\text{F.T. } \partial_{\mu} j_A^{\mu} = s_f \rho_B \frac{q_f}{\pi} \tilde{E}_{\parallel}(q) e^{-\frac{|\mathbf{q}_{\perp}|^2}{2|q_f B|}} = \frac{q_f^2}{2\pi^2} \tilde{\mathbf{E}}(q) \cdot \mathbf{B} e^{-\frac{|\mathbf{q}_{\perp}|^2}{2|q_f B|}}. \quad (17)$$

³ This pole does not exist in the massive case according to the limit (10).

Remember that \tilde{E}_{\parallel} is the component of the electric field automatically projected in the magnetic-field direction in Eq. (4b) and depends on q_{\parallel}^2 and $|\mathbf{q}_{\perp}|^2$ in general, while B is a constant strength. The same structure arises repeatedly below. This AWI (17) reproduces the chiral anomaly in the (3+1) dimensions up to the Gaussian factor. We will discuss the Gaussian factor below and put it aside at this moment.

Notice that both the divergence of the axial current and the product of the electromagnetic fields are dimension-four quantities. Therefore, the remaining factor in Eq. (17) is just a constant which is sometimes referred to as the anomaly coefficient. The same applies to the general form of Π_{\parallel} in Eq. (4b). Since Π_{\parallel} always has the overall factor of $q_f B$ from the Landau degeneracy factor, the remaining part has to be only a function of dimensionless quantities. Including all the contributions to Π_{\parallel} obtained in Eq. (14), we find that

$$\text{F.T. } \partial_{\mu} j_A^{\mu} = w(\omega, q_z) \frac{q_f^2}{2\pi^2} \tilde{\mathbf{E}}(q) \cdot \mathbf{B} e^{-\frac{|\mathbf{q}_{\perp}|^2}{2|q_f B|}}, \quad (18a)$$

$$w(\omega, q_z) := 1 - I\left(\frac{q_{\parallel}^2}{4m^2}\right) + m^2 \int_{-\infty}^{\infty} \frac{dp_z}{\epsilon_p} \frac{n_+(\epsilon_p) + n_-(\epsilon_p)}{q_{\parallel}^2 \sqrt{1 - 4m^2/q_{\parallel}^2}} \left(\frac{\epsilon_p^+ s_+}{p_z - p_z^+} - \frac{\epsilon_p^- s_-}{p_z - p_z^-} \right). \quad (18b)$$

The first term in $w(\omega, q_z)$ is the same anomalous term as in the massless case (17), so that a deviation of $w(\omega, q_z)$ from unity quantifies both the vacuum and medium contributions for massive fermions. It may be appropriate to call Eq. (18) the axial Ward identity (AWI) rather than the anomaly equation or something of this sort, because the right-hand side now has the terms other than the anomalous term. Those additional terms are identified with matrix elements of the pseudoscalar condensate, i.e., $2im\langle\bar{\psi}\gamma^5\psi\rangle$. In Appendix B, we confirm this statement with an explicit computation of the axial-vector correlator.

We summarize the limiting behaviors defined by the dimensionless combinations below and in Table 2.

- “Massless” limit $q_{\parallel}^2/m^2 \rightarrow \infty$: There is no medium correction in this limit, and the result is the same as in vacuum with massless fermions. This limit needs to be defined with a finite value of q_{\parallel}^2 that requires a nonzero energy ω and/or momentum q_z of the electric field \tilde{E}_{\parallel} along the magnetic-field direction. The absence of temperature corrections to the anomalous term was shown in the strictly massless case to all orders in the coupling constant [35].
- Adiabatic limit $q_{\parallel}^2/m^2 \rightarrow 0$ in vacuum: As explicitly shown in Sec. C, this limit

corresponds to constant electric fields. The axial current is conserved in vacuum since a massive fermion and antifermion pair cannot be created in an adiabatic process [37].

- Adiabatic limit $q_{\parallel}^2/m^2 \rightarrow 0$ in medium: The spectral flow occurs to the medium particles and gives rise to a nonzero divergence of the axial current. This is because acceleration by electric fields induces a momentum flip and thus a helicity flip when the spectral flow goes through the bottom of the parabolic dispersion relation. We will find that, in the high-temperature or density limit ($m/T, m/\mu \rightarrow 0$), the nonzero divergence takes the same form as the anomalous term in vacuum, though it arises from the mass-dependent part instead of the anomalous term.
- Diabatic processes: A nonzero energy ω and/or momentum q_z of the electric field \tilde{E}_{\parallel} allows for an axial-charge creation in diabatic processes only if fermions are massive. The relevant processes are a fermion and antifermion pair creation from a single photon and the Landau damping that is a scattering of a medium particle off a space-like photon.

Overall, one can only get simple results in the adiabatic limit which can be understood with the spectral flow. However, the flow pattern depends on the fermion mass, temperature and density. Once diabatic processes are activated, fermions do not follow the ordered collective flow. Then, one needs to investigate the frequency and wavelength dependences of the AWI with the explicit form of the response function, which do not exhibit universal

	“Massless limit” ($q_{\parallel}^2/m^2 \rightarrow \infty$)	Massive cases	
		Adiabatic limit ($q_{\parallel}^2/m^2 \rightarrow 0$)	Diabatic processes
Vacuum	$w = 1$	$w = 0$	$w \neq 0$ Pair creation
Medium	$w = 1$	$w \neq 0$ $w = 1$ in high T (μ) limit	$w \neq 0$ Pair creation & Landau damping

FIG. 2. Summary of the limiting behaviors of $w(\omega, q_z)$ that show relative magnitudes to the anomalous term. The high- T limit refers to $m/T \rightarrow 0$ and $T/\mu \gg 1$, while the high- μ limit $m/\mu \rightarrow 0$ and $T/\mu \ll 1$.

behaviors. The AWI takes the simple universal form in the massless case only because those diabatic processes are kinematically prohibited.⁴ The massless nature strongly restricts possible processes to those that occur in the right- and left-handed sectors independently [see comments below Eq. (16)].

B. Vacuum contributions

We discuss the vacuum processes that create axial charges and find that massless and massive fermions behave quite differently.

1. Massless case

The AWI (17) reproduces the chiral anomaly in (3+1) dimensions up to the Gaussian factor. The numerical factor is reproduced as a product of the Landau degeneracy factor ρ_B and the anomaly coefficient in the (1+1) dimensions, i.e., F.T. $\partial_\mu j_A^\mu = (q_f/\pi)E$ (see, e.g., Ref. [39]). This is a natural consequence of the effective dimensional reduction in the LLL. The total current is given by sum of the copies of the (1+1)-dimensional currents; Degenerate states in the momentum space correspond to the center positions of cyclotron motion in the coordinate space.

However, the wave function of the LLL has a finite extension in the transverse plane that is of the order of the cyclotron radius $1/\sqrt{|q_f B|}$. The extra Gaussian factor is a manifestation of this finite extension, and is a function of the ratio of the cyclotron radius to the transverse resolution scale $1/|\mathbf{q}_\perp|$. The Gaussian factor reduces to unity in the low-resolution limit $|\mathbf{q}_\perp|^2/|q_f B| \rightarrow 0$. We discuss the relation between the AWIs from the LLL approximation and from the familiar triangle diagrams more explicitly in Appendix C.

As well-known, the above axial-charge creation can be interpreted with the spectral-flow picture [36, 37] (see, e.g., Ref. [38, 39] for pedagogical discussions). The spectral flow refers to an adiabatic shift of the filled states along the dispersion curve in response to external electric fields, as shown in Fig. 3 for massless fermions in vacuum.

⁴ In a sense, this situation is similar to that in quantum Hall systems and/or topological insulators where clean edge currents can be measured thanks to the absence of non-universal metallic currents in the bulk. Noises are muted by inherent mechanisms.

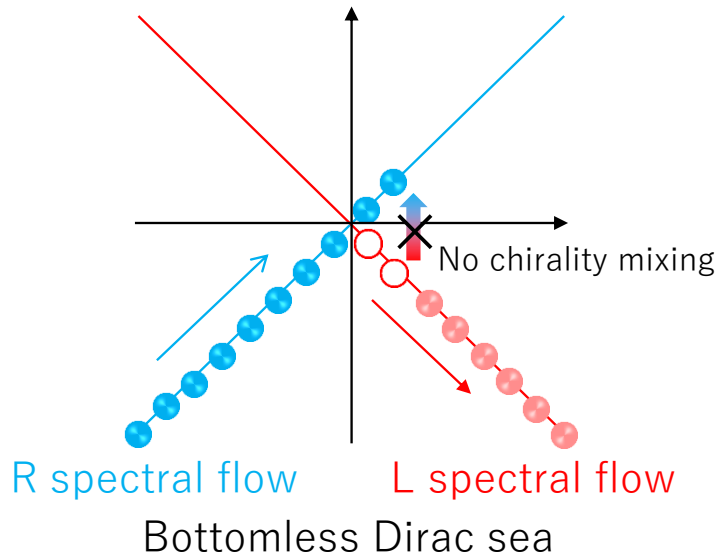


FIG. 3. Spectral flows of right- and left-handed massless fermions in vacuum.

To further apply the spectral-flow picture to the massive and/or in-medium cases, we remind the readers of two simple but crucial points. The spectral flow occurs along the dispersion relation of fermions and it occurs only when the states on the dispersion relation are occupied. Note that the fermion mass enters the dispersion relation, while temperature and/or density enters the fermion distribution function. Below, we will see that those parameters control patterns of the spectral flow and even determine whether or not the axial-vector current is effectively conserved.

In case of the strictly massless case, the dispersion relations of the right- and left-handed fermions are represented with the diagonal lines in Fig. 3. Independent spectral flows occur along the two dispersion relations since there is no chirality mixing in the massless case. While the spectral shifts do not change the occupation number in the bottomless Dirac sea due to the infinity, a finite difference manifests itself in the infrared regime in the form of the chirality production.

2. Massive case

Next, we show that the paths of the spectral flows are changed for massive fermions (cf. Fig. 4), giving rise to a drastic change in the AWI. Also, we point out that chirality mixing by a finite mass term allows for a *adiabatic* axial-charge creation.

The massive polarization function Π_{\parallel} in Eq. (8) provides the AWI

$$\text{F.T. } \partial_{\mu} j_A^{\mu} = \frac{q_f^2}{2\pi^2} \tilde{\mathbf{E}}(q) \cdot \mathbf{B} \left[1 - I\left(\frac{q_{\parallel}^2}{4m^2}\right) \right] e^{-\frac{|\mathbf{q}_{\perp}|^2}{2|q_f B|}}. \quad (19)$$

The unit term in the brackets is the same anomalous term as in the massless case (17). As explicitly identified in Appendix B, the other term is the matrix element of the pseudoscalar condensate $2im\langle\bar{\psi}\gamma^5\psi\rangle$, which automatically arises from computation of the massive fermion loop. In terms of the classical equation of motion, the origin of this term is easily identified with the explicit symmetry breaking by the fermion mass term in the Lagrangian. Nevertheless, the matrix element needs a one-loop diagram with insertion of the external photon field to take a nonzero value.

Notice that the anomalous term itself is independent of the mass scale since it originates from the ultraviolet regularization of the bottomless Dirac sea. In other words, the spectral flow from the bottom of the Dirac sea is always there. However, the magnitude of the axial-current generation, the manifestation of chiral anomaly in the infrared regime, depends on the relative magnitude to the pseudoscalar-condensate term that depends on the fermion mass.

One can discuss the adiabatic limit such that $q_{\parallel}^2/m^2 \rightarrow 0$, where there is no invariant energy transfer from the electric field. This configuration corresponds to a constant electric field that is time-independent and homogeneous along the magnetic-field direction (see Appendix C for more explicit explanations). Note that the electric field can still have an inhomogeneity in the transverse plane when $|\mathbf{q}_{\perp}|$ is finite, giving the Gaussian factor. In the adiabatic limit, we have $I(0) = 1$, so that the axial current is conserved, i.e.,

$$\lim_{q_{\parallel}^2/m^2 \rightarrow 0} \text{F.T. } \partial_{\mu} j_A^{\mu} = 0. \quad (20)$$

This is a natural result because the weak electric field, perturbatively applied in Eq. (4b), cannot create massive on-shell fermions in an *adiabatic* process. Any finite value of mass corresponds to the “infinite mass” limit in the relative sense $q_{\parallel}^2/m^2 \rightarrow 0$. This explains why the above result is independent of the fermion mass; Unity ($= m^2/m^2$) is the only one possible dimensionless combination when $q_{\parallel}^2 \rightarrow 0$. The massless limit should be taken with a finite value of q_{\parallel}^2 as $q_{\parallel}^2/m^2 \rightarrow \infty$, reproducing the massless limit (17) with $I(\infty) = 0$.

As clear in the above derivation (cf. Appendix B as well), the conservation of the axial current (20) simply means that a far-off-shell fermion loop vanishes when the fermion mass

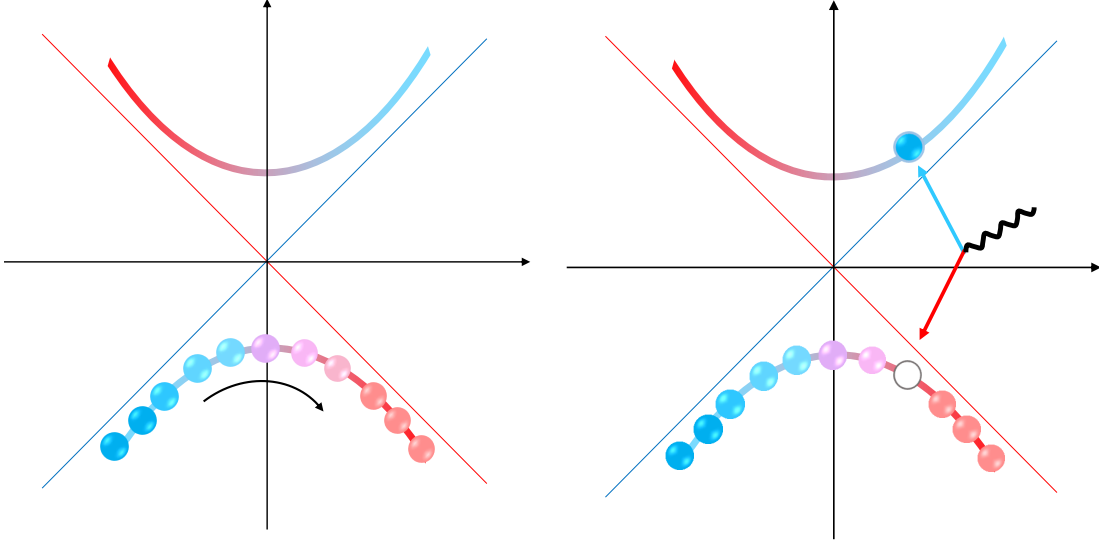


FIG. 4. Adiabatic spectral flow of massive fermions in vacuum (left) and diabatic massive pair creation from a single photon in vacuum (right).

is much larger than any of external momenta, $q_{\parallel}^2/m^2 \rightarrow 0$. Also, one can understand the conservation of the axial current in terms of the spectral flow along the parabolic curve in Fig. 4 (left). Since the positive- and negative-energy states are separated by the mass gap, the adiabatic spectral flow turns back to the bottom of the Dirac sea, creating no axial charge [37, 45]. This flow pattern is in a clear contrast to the massless case in Fig. 3. Below, we find that the medium contribution gives rise to an additional spectral flow.

In diabatic processes, a finite axial charge can be created with a finite energy transfer ($q_{\parallel}^2/m^2 \neq 0$) from non-constant electric fields. Remember that a fermion and antifermion pair can be created from a single photon in strong magnetic fields as discussed in Paper I. This process is possible only for massive fermions because the created pair has the same helicity along the magnetic field, requiring a chirality mixing at the vertex (see Appendix A for summary of the quantum numbers that specify the LLL fermions and antifermions). Once the process occurs, the created pair carries a net helicity, giving rise to a nonzero contribution to the AWI.⁵

Figure 4 (right) exhibits a pair creation from a single photon. The chirality mixing by a finite fermion mass is expressed with a color gradient from red to blue. The mixing strength is maximum at $p_z = 0$, and the fermion wave function approaches the chirality eigenstate

⁵ This can be understood from kinematics in the center-of-momentum frame of the pair where the momenta of a pair is in the back-to-back direction. The spin directions are also oriented in the opposite directions along the magnetic field due to the large Zeeman energy. Thus, the pair has the same helicity.

in the large momentum regime $|p_z|/m \gg 1$. Therefore, when a created fermion is right-ish (left-ish) in chirality, an antiparticle can be left-ish (right-ish), creating a finite axial charge. The back-to-back kinematics is only allowed for massive fermions with this chirality mixing, and the diabatic pair creation is prohibited in the massless case. A similar prohibition mechanism is known as the “helicity suppression” in the leptonic decay of charged pions [46, 47].

C. Medium contributions

1. Spectral flow in medium

Next, we consider the medium contributions. In contrast to the vacuum case, even a soft photon can perturb the systems when medium fermions are populated in the positive-energy states above the mass gap at finite temperature and/or density. In this case, the axial current will not be conserved if scatterings with single photons induce helicity flips. Including the medium contribution to Π_{\parallel} obtained in Eq. (14), we find the AWI (18). Again, there is no correction to the anomalous term itself since the medium corrections do not change the (superficial) UV divergence. The medium part, proportional to the fermion mass, can be identified with the medium correction to the matrix element of the pseudoscalar condensate. Namely, including the medium correction, the pseudoscalar condensate in the LLL reads

$$2im\langle\bar{\psi}\gamma^5\psi\rangle = \frac{q_f^2}{2\pi^2}\tilde{\mathbf{E}}(q)\cdot\mathbf{B}e^{-\frac{|\mathbf{q}_{\perp}|^2}{2|q_f B|}}[w(\omega, q_z) - 1], \quad (21)$$

with $w(\omega, q_z)$ defined in Eq. (18). Those terms vanish in the massless limit, i.e., $w(\omega, q_z) \rightarrow 1$, and the AWI (18) goes back to that in the massless limit (17).

We first discuss a drastic change in the spectral flow. In contrast to the vacuum case where the spectral flow of massive fermions does not generate an axial charge [cf. Eq. (20)], the spectral flows of medium particles can create axial charges as illustrated in Fig. 5. Notice that the Fermi-Dirac distribution function works as a finite cutoff to the loop momentum. This makes a big difference from the vacuum spectral flow beneath the *bottomless* Dirac sea (see Fig. 4 and the discussions there).

In the presence of the thermal cutoff, a state just above the thermal cutoff is filled after the spectral flow on the positive-energy branch and a previously occupied state just below the thermal cutoff is removed on the other wing of the parabolic dispersion curve

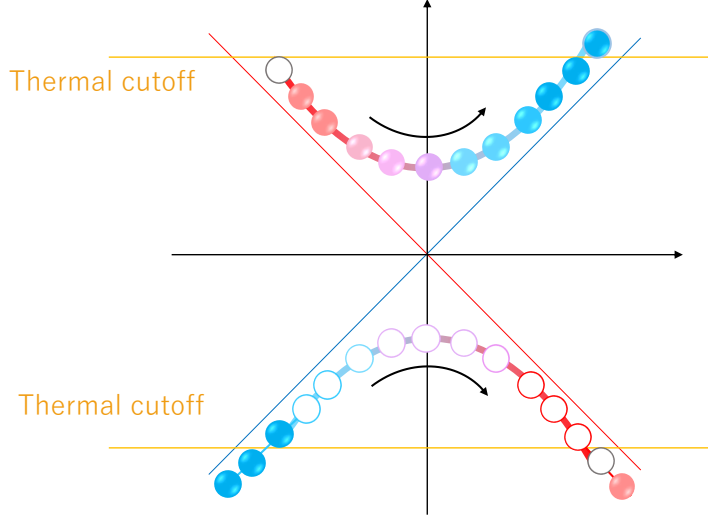


FIG. 5. Spectral flows of massive fermions and antifermions (shown as holes) in medium.

(cf. Fig. 5). This process of course does not change the total particle number, but changes the helicity. What happens during this process is a momentum flip, and thus a helicity flip, across the “valley” of the parabolic dispersion curve. The same occurs in the positive-energy antiparticle branch, creating a net axial charge. This axial-charge creation is not anomalous in the sense that its origin is not related to the concept of infinity known with the “Hilbert hotel” [48].

Indeed, the above axial-charge creation originates not from the anomalous term but from the mass-dependent pseudoscalar condensate term. Remarkably, the result will turn out to have the same form as the anomalous term in the adiabatic and high-temperature limits (or in the adiabatic and high-density limits). This is simply because the axial-charge imbalance appears near the thermal cutoff instead of the infrared regime, so that effects of the finite curvature along the dispersion curve is negligible in the high-temperature or high-density limit defined as $m/T, m/\mu \rightarrow 0$.

To verify the above statements, we examine the zero frequency and momentum limits. Though the results turn out to be independent of the ordering of the limits, one can consider the following two orderings:

$$\lim_{\omega/m \rightarrow 0} \lim_{q_z/m \rightarrow 0} \text{F.T. } \partial_\mu j_A^\mu = \frac{q_f^2}{2\pi^2} \tilde{\mathbf{E}}(q) \cdot \mathbf{B} e^{-\frac{|\mathbf{q}_\perp|^2}{2|q_f B|}} \lim_{\omega/m \rightarrow 0} 2m^2 \mathcal{P} \int_{-\infty}^{\infty} \frac{dp_z}{\epsilon_p} \frac{n_+(\epsilon_p) + n_-(\epsilon_p)}{(2\epsilon_p)^2 - \omega^2}, \quad (22a)$$

$$\lim_{q_z/m \rightarrow 0} \lim_{\omega/m \rightarrow 0} \text{F.T. } \partial_\mu j_A^\mu = \frac{q_f^2}{2\pi^2} \tilde{\mathbf{E}}(q) \cdot \mathbf{B} e^{-\frac{|\mathbf{q}_\perp|^2}{2|q_f B|}} \lim_{q_z/m \rightarrow 0} \left(-\frac{m^2}{q_z} \right) \mathcal{P} \int_{-\infty}^{\infty} \frac{dp_z}{\epsilon_p} \frac{n_+(\epsilon_p) + n_-(\epsilon_p)}{p_z - \frac{1}{2}q_z},$$

(22b)

where \mathcal{P} denotes the principal value. The vacuum contribution vanishes in these limits according to Eq. (10). We have encountered the same integrals in Sec. IV of Paper I when computing the photon masses, where the orderings do matter. The distribution functions can be simply replaced by the upper and lower boundaries of the integrals in the high- T or high- μ limit, leading to simple results

$$\lim_{\Lambda/m \rightarrow \infty} \lim_{\omega/m \rightarrow 0} 2m^2 \mathcal{P} \int_{-\Lambda}^{\Lambda} \frac{dp_z}{\epsilon_p} \frac{1}{(2\epsilon_p)^2 - \omega^2} = 1, \quad (23a)$$

$$\lim_{\Lambda/m \rightarrow \infty} \lim_{q_z/m \rightarrow 0} \left(-\frac{m^2}{q_z} \right) \mathcal{P} \int_{-\Lambda}^{\Lambda} \frac{dp_z}{\epsilon_p} \frac{1}{p_z - \frac{1}{2}q_z} = 1, \quad (23b)$$

where $\Lambda = T$ or μ . Note that a hierarchy $T/\mu \gg 1$ ($T/\mu \ll 1$) needs to be satisfied for the above replacement, in addition to the high-temperature limit $m/T \rightarrow 0$ (high-density limit $m/\mu \rightarrow 0$). Plugging the above integrals into Eq. (22), one finds the AWI in the adiabatic and high-temperature (or high-density) limits

$$\lim_{\omega/m \rightarrow 0} \lim_{q_z/m \rightarrow 0} \text{F.T. } \partial_\mu j_A^\mu = \lim_{q_z/m \rightarrow 0} \lim_{\omega/m \rightarrow 0} \text{F.T. } \partial_\mu j_A^\mu = \frac{q_f^2}{2\pi^2} \tilde{\mathbf{E}}(q_\perp) \cdot \mathbf{B} e^{-\frac{|\mathbf{q}_\perp|^2}{2|q_f B|}}. \quad (24)$$

Notice that the medium contribution to the pseudoscalar condensate results in the same form as the anomalous term. This mechanism is rather similar to the “chiral anomaly” in lattice models; The approximate linear dispersion relations are connected with each other as segments of the periodic dispersion relations, forming a valley similar to Fig. 5. In short, we have explicitly seen that the axial charge is generated by the spectral flow of thermally populated fermions even when the spectral flow beneath the Dirac sea cannot contribute at all.

2. *Adiabatic processes*

When the electric field has a finite frequency ω , the pair creation and the Landau damping can contribute to the integral in Eq. (21). The electric field can be both external one and of a dynamical photon as long as its magnitude is perturbatively weak. According to the optical theorem, nonzero rates of those reactions are directly captured by the imaginary part of the polarization tensor that gives a real part of the induced axial current just like electric currents are expressed by imaginary parts of the retarded correlators according to the Kubo

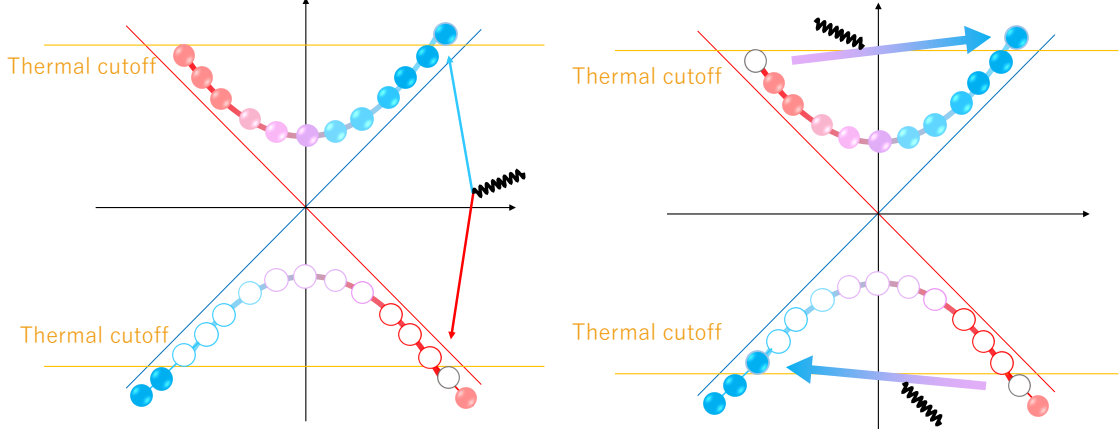


FIG. 6. Axial-charge creation from the pair creation (left) and the Landau damping (right).

formula.⁶ The real part of the polarization tensor also exhibits peak structures originating from those reactions (see Sec. III. B in Paper I); The real and imaginary parts are related to each other via the dispersion integral, and are two sides of the same coin.

Kinematics in the relevant processes are shown in Fig. 6. We have discussed the contribution from the pair creation in Sec. IV B 2 in vacuum case. The medium correction should suppress the pair creation due to the Pauli-blocking effect in the final state when the photon energy is smaller than the temperature and/or density scale. On the other hand, the Landau damping is a pure medium effect in which a medium fermion is scattered off an off-shell photon. The scatterings from one side to the other side of the parabolic dispersion relation is accompanied by a helicity flip. We have inspected those reactions in Paper I by performing the same integral as that in Eq. (21).

To understand basic behaviors of $w(\omega, q_z)$ defined in Eq. (18), we consider the homogeneous limit ($q_z \rightarrow 0$)

$$\lim_{q_z/m \rightarrow 0} w(\omega, q_z) = 1 - I\left(\frac{\omega^2}{4m^2}\right) + 2m^2\mathcal{P} \int_{-\infty}^{\infty} \frac{dp_z}{\epsilon_p} \frac{n_+(\epsilon_p) + n_-(\epsilon_p)}{(2\epsilon_p)^2 - \omega^2}, \quad (25)$$

where the electric field may still have a transverse inhomogeneity $|\mathbf{q}_\perp| \neq 0$. The left panel in Fig. 7 shows the real and imaginary parts of $w(\omega)$ with blue and red lines, respectively. The colored dashed lines show the vacuum contributions. The adiabatic limit corresponds to the interception at $\omega = 0$ that vanishes in vacuum as discussed above, but takes finite values in medium. We compare the low- and high-temperature cases with $T/m = 0.5$ (darker color)

⁶ Note that we take the divergence of the axial current in the present case, which adds a complex unit and a momentum factor.

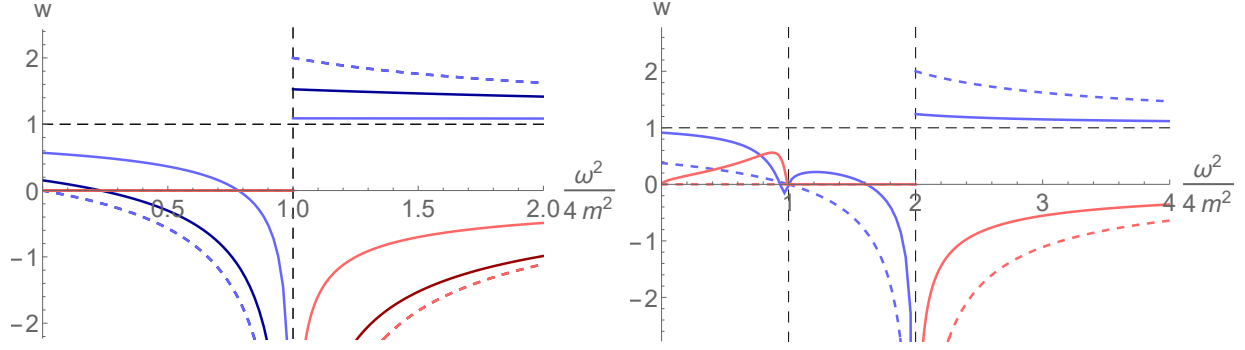


FIG. 7. $w(\omega, q_z)$ for the AWI at $q_z = 0$ in the homogeneous limit [left] and at $q_z/(2m) = 1$ [right]. The blue and red lines show the real and imaginary parts, respectively. We take temperature scales $T/m = 0.5$ (the darker colors) and $T/m = 1.5$ (the lighter colors) at zero density ($\mu = 0$), while the vacuum contribution is shown with dashed lines.

and $T/m = 1.5$ (lighter color) at zero density $\mu/m = 0$. As we increase temperature, the real part approaches the constant value $w(\omega) = 1$ in the massless limit. The imaginary part above the threshold, on the right of the dashed vertical line, gives the contribution from the pair creation. The imaginary part diverges as ω approaches the threshold from above. Correspondingly, the real part also diverges as ω approaches the threshold from below. Those behaviors are typical threshold behaviors in (1+1) dimensions and manifest themselves here because of the effective dimensional reduction in the strong magnetic fields. The sign of the real part depends on ω , which is due to a phase lag in response to time-dependent electric fields.

In the right panel of Fig. 7, we show the AWI at a finite value of momentum $q_z/(2m) = 1$. We take $T/m = 1.5$ and $\mu/m = 0$ as in the left panel. When ω is small, there is a spatial region $\omega^2 - q_z^2 < 0$ on the leftmost side of the dashed vertical lines. In this region, the imaginary part, shown with the red line, solely stems from the Landau damping. In the adiabatic or stationary limit ($\omega \rightarrow 0$), the imaginary part, however, vanishes for any value of q_z since imaginary parts of retarded correlators are odd functions of ω on the general ground. There appears a negative peak structure in the real part corresponding to the peak structure in the imaginary part. Qualitative behaviors in the other regions are common to the left panel at $q_z = 0$. Both the real and imaginary parts go through the point $w(\omega = q_z, q_z) = 0$ where $q_{\parallel}^2 = 0$.

Finally, we show the AWI at zero temperature and a finite chemical potential $\mu/m = 2$

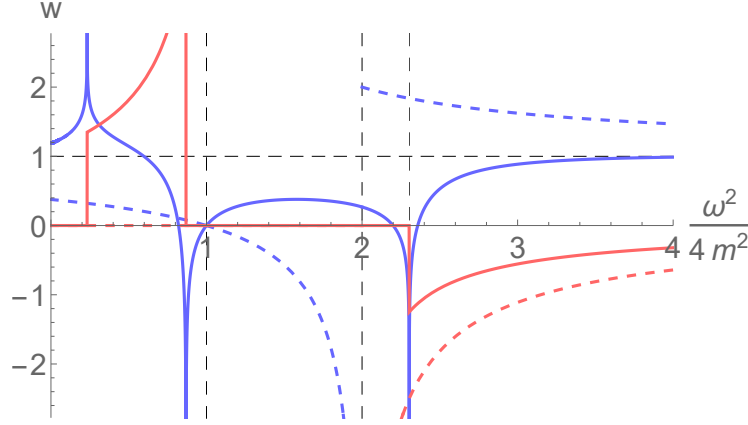


FIG. 8. $w(\omega, q_z)$ for the AWI at zero temperature and a finite chemical potential $\mu/m = 2$. We take $q_z/(2m) = 1$ as in Fig. 7.

in Fig. 8. We take $q_z/(2m) = 1$ as in Fig. 7. Remarkably, the diverging threshold behavior at $q_{\parallel}^2 = 4m^2$ shifts to a higher energy. This is due to the Pauli-blocking effect; Since the positive-energy states are occupied up to the sharp Fermi surface, the pair creation can only occur in vacant states above the Fermi surface, requiring a larger energy of the order of the chemical potential. The singular behaviors at the threshold is now logarithmic and the threshold position splits into this one and a higher one that is outside the plot region (see Paper I for more discussions). The Landau damping also gives rise to step singularities in the imaginary part since it brings one occupied state below the sharp Fermi surface to a vacant state above the Fermi surface. Finite-temperature effects make vacancy below the Fermi surface, so that the threshold position goes back to $q_{\parallel}^2 = 4m^2$ at finite temperature.

V. SUMMARY AND DISCUSSIONS

In this paper, we investigated the AWI in the LLL approximation that is composed of the anomalous and pseudoscalar-condensate terms. The AWI is saturated by the anomalous term in the massless case irrespective of the presence or absence of the medium. The polarization tensor, the central quantity in this series of papers, describes the medium corrections to the pseudoscalar condensate which, therefore, should be proportional to the fermion mass. We showed how the AWI as a whole behaves when we vary temperature and/or density as well as the fermion mass and the external photon momentum. We classified the mechanisms of the axial-charge generation into the adiabatic and diabatic processes.

For the adiabatic processes, we further classified the patterns of the spectral flows putting an emphasis on two simple points, that is, the shape of dispersion relation and whether or not the states on the dispersion relation are occupied. The spectral flows take the paths along the dispersion relations, and thus there is a qualitative difference between the massless and massive cases. A nonzero axial charge could only stem from the spectral flow of the positive-energy states in the massive case since the anomalous term is offset by the vacuum part of the pseudoscalar condensate in the adiabatic limit. Therefore, a nonzero axial charge is generated by the helicity flip on the medium particles and does not contain a contribution from the anomalous term; The AWI is dominated by the medium contribution. It is remarkable that the medium contribution, nevertheless, agrees with the anomalous term in the high-temperature or high-density limit as compared to the fermion mass, where the curvature of the parabolic dispersion relation is negligible. We showed those limiting behaviors in an analytic way and would like to add that there are possible contributions from the higher Landau levels in such limits, which needs to be investigated in the future works.

We also investigated the diabatic contributions to the axial-charge generation which can be finite only for massive fermions. The relevant physical processes are the pair creation from a single photon and the Landau damping. Those processes are not anomalous in the sense that they are nothing to do with the ultraviolet divergence. Thus, there are possible higher-order radiative corrections. Such corrections in QED may be small in many of relevant applications in vacuum. However, when scatterings with medium particles happen so frequently in high-energy-density states, such corrections can be significant even in weak-coupling theories. In addition, there are possible contributions from the higher Landau levels. Remember that the AWIs from the LLL approximation and the triangle diagrams only agree with each other in the homogeneous limit $|\mathbf{q}_\perp|^2/|q_f B| \rightarrow 0$ as explicitly shown in Appendix C. The discrepancy needs to be compensated by contributions from the higher Landau levels, and can be significant when the higher Landau levels are excited at the temperature and/or density scale comparable to the magnetic-field strength. Such environments can be realized in relativistic heavy-ion collisions, neutron star, and the early universe depending on detailed situations. We leave those points and applications as future works.

Studying the axial-charge dynamics provides implications for various systems. The amount of the created axial charge determines the magnitude of the CME currents induced in relativistic heavy-ion collisions [4–6, 19] and the Weyl and Dirac semimetals [7–9]. The

axial-charge dynamics even plays a crucial role when the magnetic fields are dynamical and are subject to the chiral plasma instability that has been discussed as a possible origin of the strong magnetic fields in the early universe and neutron stars/magnetars [10, 13–18, 49]. The time evolution of the axial-charge density should be tracked consistently coupled to the amplification of the magnetic fields. In addition to those CME-induced phenomena, one can study the axial-charge dynamics revealing itself in the optical activities. Such directions have been pursued with the Weyl and Dirac semimetals [50–66]. It is interesting to investigate possible optical signals from the quark-gluon plasma and from the outer space as well.

There is another implication for the production of axion or any hypothetical pseudoscalar particles via the Primakoff effect [67–71]. This mechanism can be understood as a mixing process between a single photon and the single pseudoscalar particle in strong magnetic fields of stars or galaxies. The similar idea leads to the light-shining-through-wall experiment in laboratories (see, e.g., Refs. [72, 73] for reviews). The two-point function between the axial and vector currents studied in this paper determines the mixing strength with the inclusion of the screening effect in medium. The screening effect can be important in stars and galaxies, giving rise to the nontrivial peak structures in the photon-energy and -momentum dependences shown in this paper. This deserves further studies in fundamental physics.

Acknowledgments.— KH thanks Patrick Copinger, Kenji Fukushima, Yoshimasa Hidaka, Xu-Guang Huang, Hidetoshi Taya, and Di-Lun Yang for discussions. This work is supported in part by JSPS KAKENHI under grant Nos. 20K03948 and 22H02316.

Appendix A: Massless fermions and antifermions in the LLL

We summarize the quantum numbers characterizing the LLL fermions and antifermions to clarify somewhat confusing terminologies. For clarity, we here assign the following terminologies.

“Chirality” is an eigenvalue of γ^5 that specifies the handedness of the spinor $\psi_{R/L}$, i.e., $\gamma^5\psi_{R/L} = \pm\psi_{R/L}$ with the upper/lower signs for R/L . “Axial charge” is the difference between the number densities $j_A^0 = n_R - n_L$ created by the spinors $\psi_{R/L}$. Since antiparticles are counted in the net number densities with negative signs, they contribute to the axial charge

with opposite signs to the particle contributions. Those correspondences are summarized in Table I.

“Helicity” is defined by the relative direction between spin and momentum as $h = S_z p_z / |p^0|$ with the spin operator $S_z = i\gamma^1\gamma^2/2$. The correspondence to chirality is made clear if one refers to the Dirac operator. The fermion spinor ψ_{LLL} for the LLL should satisfy the following Dirac equation (see Paper I)

$$(p^0 - s_f p_z \gamma^5) \psi_{\text{LLL}} = 0, \quad (\text{A1})$$

where we used the fact that the LLL spinor is an eigenfunction of the spin operator $2S_z \psi_{\text{LLL}} = (i\gamma^1\gamma^2) \psi_{\text{LLL}} = s_f \psi_{\text{LLL}}$. Therefore, one finds that

$$h \psi_{\text{LLL}} = \frac{1}{2} \text{sgn}(p^0) \gamma^5 \psi_{\text{LLL}}, \quad (\text{A2})$$

where $(\gamma^5)^2 = 1$. The relative sign between the chirality and the helicity depends on the sign of the energy. Therefore, ψ_{LLL}^R (ψ_{LLL}^L) contains the right-handed helicity particles and left-handed helicity antiparticles (the left-handed helicity particles and right-handed helicity antiparticles). The particles and (positive-energy) antiparticles should have opposite helicities because they move in the same directions but have opposite spin directions due to the Zeeman effect. Helicity is independent of the sign function s_f , because both the spin and momentum directions depend on s_f .⁷

Massive fermions are none of those eigenstates, and are the mixed states of them as shown in Figs. 4 and 5 with the color gradient. Some scattering processes require such chirality mixing to occur with finite amplitudes.

TABLE I. Quantum numbers that specify the massless LLL fermions and antifermions. The upper and lower signs are for the right- and left-handed chirality sectors, respectively.

	Spin (S_z)	Chirality (γ^5)	Axial charge (j_A^0)	Momentum (p_z)	Helicity ($S_z p_z / p_z $)
Particles	$s_f \frac{1}{2}$	± 1	± 1	$\pm s_f$	$\pm \frac{1}{2}$
Antiparticles	$-s_f \frac{1}{2}$	± 1	∓ 1	$\pm s_f$	$\mp \frac{1}{2}$

⁷ Notice that the Dirac equation (A1) is satisfied with the dispersion relations $p^0 = \pm s_f p_z$ *without* the symbol of absolute value. The upper and lower signs are for the right- and left-handed chirality eigenstates, respectively, and should not be mixed up with the signs for positive- and negative-energy solutions. The sign of p^0 depends on that of p_z .

Appendix B: Chiral anomaly diagram with massive LLL fermions

In this Appendix, we directly compute the anomaly diagram with massive fermions in the LLL and demonstrate that it splits into the anomalous term and the matrix element of the pseudoscalar condensate. One can also explicitly confirm that the anomalous term is independent of the fermion mass, while the latter is proportional to the fermion mass required by the chirality mixing in the pseudoscalar fermion bilinear.

We examine the two-point function composed of the LLL fermion loop:

$$\int d^4x e^{-iqx} \langle k | \partial_\mu j_A^\mu(x) | 0 \rangle = \rho_B e^{-\frac{|q_\perp|^2}{2|q_f B|}} (2\pi)^2 \delta^{(2)}(k_\parallel - q_\parallel) i q_\mu \Pi_{1+1(A)}^{\mu\nu}(q_\parallel) \epsilon_\nu^*(q). \quad (\text{B1})$$

The Landau degeneracy factor and the Gaussian come from the transverse-momentum integral as in the computation of the vector-current correlator (cf. Paper I). The residual (1+1)-dimensional longitudinal part is given as

$$i q_\mu \Pi_{1+1(A)}^{\mu\nu}(q_\parallel) = (-1)(-i q_f) \int \frac{d^2 p_\parallel}{(2\pi)^2} \frac{\text{tr}[\not{q}_\parallel \gamma^5 i(\not{p}_\parallel + m) \mathcal{P}_+ \gamma_\parallel^\nu i(\not{p}_\parallel + \not{q}_\parallel + m) \mathcal{P}_+]}{(p_\parallel^2 - m^2)((p_\parallel + q_\parallel)^2 - m^2)}. \quad (\text{B2})$$

The two-dimensional integral has a (superficial) logarithmic divergence, and we use the dimensional regularization.

It is important to make sure the properties of the γ^5 to apply the dimensional regularization. The γ^5 is extended in such a way that $\{\gamma^5, \gamma^\mu\} = 0$ for $\mu = 0, 1, 2, 3$ and $[\gamma^5, \gamma^\mu] = 0$ for the other extra components. The extra components in the momentum is denoted with tilde like $\tilde{\ell}^\mu$, which corresponds to ℓ_\perp^μ in the notations of Ref. [39].⁸ The external momenta q^μ, k^μ have vanishing components in the extra dimensions, $\tilde{q}^\mu = \tilde{k}^\mu = 0$. The extra components of γ^μ commute with γ^5 , i.e., $[\tilde{\ell}, \gamma^5] = 0$. Then, one can show an identity

$$\not{q}_\parallel \gamma^5 = \gamma^5 (\not{p}_\parallel - m) + (\not{q}_\parallel + \not{p}_\parallel - m) \gamma^5 + 2(m - \tilde{p}_\parallel) \gamma^5. \quad (\text{B3})$$

Plugging the identity (B3) into the (1+1)-dimensional part, we have

$$\begin{aligned} i q_\mu \Pi_{1+1(A)}^{\mu\nu}(q_\parallel) \epsilon_\nu^*(q) &= q_f \epsilon_\nu^*(q) \int \frac{d^d p_\parallel}{(2\pi)^d} \left[\frac{\text{tr}[\gamma^5 \mathcal{P}_+ \gamma_\parallel^\nu (\not{p}_\parallel + \not{q}_\parallel + m)]}{(p_\parallel + q_\parallel)^2 - m^2} + \frac{\text{tr}[\gamma^5 \mathcal{P}_+ (\not{p}_\parallel + m) \gamma_\parallel^\nu]}{p_\parallel^2 - m^2} \right] \\ &\quad - 2 q_f \epsilon_\nu^*(q) \int \frac{d^d p_\parallel}{(2\pi)^d} \frac{\text{tr}[\tilde{p}_\parallel \gamma^5 (\not{p}_\parallel + m) \mathcal{P}_+ \gamma_\parallel^\nu (\not{p}_\parallel + \not{q}_\parallel + m) \mathcal{P}_+]}{(p_\parallel^2 - m^2)((p_\parallel + q_\parallel)^2 - m^2)} \\ &\quad + 2im \langle \bar{\psi} \gamma^5 \psi \rangle. \end{aligned} \quad (\text{B4})$$

⁸ We do not use their notations with \parallel, \perp to avoid possible confusions with the parallel and perpendicular components with respect to the magnetic field in the present paper.

Each of the two terms in the square brackets vanishes because the integral and trace vanish if one picks up the momentum and mass factors in the trace, respectively. The last term is identified with the matrix element of the pseudoscalar condensate

$$\langle \bar{\psi} \gamma^5 \psi \rangle = (-1)[-iq_f \epsilon_\nu^*(q)] \int \frac{d^2 p_\parallel}{(2\pi)^2} \frac{\text{tr}[\gamma^5 i(\not{p}_\parallel + m) \mathcal{P}_+ \gamma_\parallel^\nu i(\not{p}_\parallel + \not{q}_\parallel) + m) \mathcal{P}_+]}{(p_\parallel^2 - m^2)((p_\parallel + q_\parallel)^2 - m^2)}. \quad (\text{B5})$$

This is the leading nonvanishing contribution from the diagram with one-insertion of the external photon leg. The remaining term in Eq. (B4) will result in the anomalous term.

We shall first examine the anomalous term. Introducing the Feynman parameter, one can make a complete square in the denominator $x(p_\parallel^2 - m^2) + (1-x)((p_\parallel + q_\parallel)^2 - m^2) = \{p_\parallel + (1-x)q_\parallel\}^2 - \Delta_\parallel$ with $\Delta_\parallel = m^2 - x(1-x)q_\parallel^2$. We then shift the integral variable as $p'_\parallel = p_\parallel + (1-x)q_\parallel$ that is allowed after the divergence is regularized. To have a nonvanishing trace, one should pick up $\gamma^1 \gamma^2$ in \mathcal{P}_+ . To have a nonvanishing integral for the extra dimension, one needs to pick up one \not{p}_\parallel from the propagator. Then, one needs to take the photon momentum \not{q}_\parallel in the other fermion propagator to make both the trace and integral nonvanishing. Therefore, assuming the presence of the integral, we have

$$\text{tr}[\tilde{\not{p}}_\parallel \gamma^5 (\not{p}_\parallel - (1-x)\not{q}_\parallel + m) \mathcal{P}_+ \gamma_\parallel^\nu (\not{p}_\parallel + x\not{q}_\parallel + m) \mathcal{P}_+] = -2s_f q_{\parallel\mu} \epsilon^{\mu\nu 12} \tilde{p}_\parallel^2. \quad (\text{B6})$$

The mass dependence as well as the Feynman parameter go away from the trace. Then, the momentum integral reads

$$\int \frac{d^d p_\parallel}{(2\pi)^d} \frac{\tilde{p}_\parallel^2}{(p_\parallel^2 - \Delta_\parallel)^2} = \frac{d-2}{d} \times \frac{(-1)i}{(4\pi)^{d/2}} \frac{d}{2} \frac{\Gamma(-\frac{d-2}{2})}{\Gamma(2)} \Delta_\parallel^{\frac{d-2}{2}} = \frac{i}{4\pi}, \quad (\text{B7})$$

where we used $(d-2)\Gamma(-\frac{d-2}{2}) = -2 + \mathcal{O}(d-2)$. The integral is finite because of the overall dimensional factor $(d-2)$. All the subleading terms vanish thanks to the same overall factor, and thus the integral is given by the above universal form. Then, we obtain the (1+1) dimensional AWI

$$iq_\mu \Pi_{1+1(A)}^{\mu\nu}(q_\parallel) \epsilon_\nu^*(k) = -\frac{q_f}{\pi} \langle k | \tilde{E}_\parallel | 0 \rangle + 2im \langle \bar{\psi} \gamma^5 \psi \rangle, \quad (\text{B8})$$

where the momentum conservation in Eq. (B1) is understood (with the delta function suppressed). As in Eq. (4), the Fourier spectrum of the electric field is defined as $\tilde{E}_\parallel(q) = -i\epsilon_\parallel^{\mu\nu} q_\mu A_\nu$ with $\epsilon_\parallel^{\mu\nu} = \epsilon^{\mu\nu 12}$.

Next, we compute the pseudoscalar condensate

$$\langle \bar{\psi} \gamma^5 \psi \rangle = \frac{s_f q_f}{2} \epsilon_\nu^*(q) \int_0^1 dx \int \frac{d^2 p_\parallel}{(2\pi)^2} \frac{\text{tr}[\gamma^5 \gamma^1 \gamma^2 (\not{p}_\parallel - (1-x)\not{q}_\parallel + m) \gamma_\parallel^\nu (\not{p}_\parallel + x\not{q}_\parallel + m)]}{(p_\parallel - \Delta_\parallel)^2}. \quad (\text{B9})$$

The integral is finite. One needs to take $\gamma^1\gamma^2$ in \mathcal{P}_+ because four gamma matrices are required for a nonzero result of the trace with one γ^5 . For the same reason, one needs to pick up one mass term, reflecting the fact that the chirality needs to be flipped. Then, there is no room for \not{p}_\parallel to be included so that the integral becomes nonvanishing. Therefore, the trace under the momentum integral reads

$$\text{tr}[\gamma^5\gamma^1\gamma^2(\not{p}_\parallel - (1-x)\not{q}_\parallel + m)\gamma_\parallel^\nu((\not{p}_\parallel + x\not{q}_\parallel) + m)] = m\text{tr}[\gamma^5\gamma^1\gamma^2\gamma_\parallel^\nu\not{q}_\parallel]. \quad (\text{B10})$$

The matrix element of the pseudoscalar condensate is proportional to the fermion mass because the pseudoscalar fermion bilinear mixes the chirality, requiring that the mass term induce chirality mixing odd times on the loop diagram.

The x -dependent terms cancel away. The remaining elementary integrals are performed as

$$\int_0^1 dx \int \frac{d^2 p_\parallel}{(2\pi)^2} \frac{1}{(p_\parallel - \Delta_\parallel)^2} = \frac{i}{4\pi} \int_0^1 \frac{dx}{m^2 - x(1-x)q_\parallel^2} = \frac{i}{4\pi m^2} I\left(\frac{q_\parallel^2}{4m^2}\right), \quad (\text{B11})$$

yielding the I function defined in Eq. (9). Thus, the matrix element of the pseudoscalar condensate is given as

$$2im\langle\bar{\psi}\gamma^5\psi\rangle = \frac{s_f q_f}{\pi} \tilde{E}_\parallel(q) I\left(\frac{q_\parallel^2}{4m^2}\right). \quad (\text{B12})$$

Combining the anomalous term and pseudoscalar condensate in Eq. (B8) reproduces the AWI (19) obtained from the polarization function Π_\parallel in Eq. (8). Explicitly, we have obtained

$$\text{F.T. } \partial_\mu j_A^\mu = \frac{q_f^2}{2\pi^2} \tilde{\mathbf{E}}(q) \cdot \mathbf{B} \left[1 - I\left(\frac{q_\parallel^2}{4m^2}\right) \right] e^{-\frac{|\mathbf{q}_\perp|^2}{2|q_f \mathbf{B}|}}. \quad (\text{B13})$$

We emphasize that both the mass-independent anomalous term and the mass-dependent pseudoscalar condensate originate from the same diagram composed of the massive fermion loop. The massive fermion loop vanishes as a whole in the large-mass limit, $\lim_{x \rightarrow 0} I(x) = 1$. This clearly explains the vanishing behavior observed below Eq. (19).

Appendix C: Relation to the triangle diagrams

Finally, we would like to establish an explicit connection between the AWI (19) from the LLL approximation and the perturbative one from the familiar triangle diagrams (cf. Fig 1). The triangle diagrams are perturbatively computed in the linear orders in the

electric- and magnetic-field strengths and contains the ABJ anomaly in (3+1) dimensions [32, 33]. On the other hand, the LLL approximation only appears after the resummation of one-loop diagrams to all orders with respect to insertion of the external legs for the constant magnetic field; The all-order resummation gives the fermion propagator the pole positions at the Landau levels. Thus, the triangle diagrams are contained in the resummed series but does not exactly correspond to the one-loop polarization tensor in the LLL. It is a non-trivial issue how the LLL approximation and the triangle diagrams are connected with each other, though the ABJ anomaly in (3+1) dimensions is often explained as a product of the Landau degeneracy factor and the (1+1) dimensional anomaly in the LLL [36]. In this appendix, we explicitly discuss their connection including the pseudoscalar-condensate term, focusing on zero temperature and density case.

Computing the massive triangle diagrams in Fig. 1, one finds the AWI [32]

$$\begin{aligned} \text{F.T. } \langle p, k | \partial_\mu j_A^\mu | 0 \rangle &= \frac{q_f^2}{2\pi^2} \cdot \frac{1}{2} [\tilde{\mathbf{E}}(k) \cdot \tilde{\mathbf{B}}(p) + \tilde{\mathbf{B}}(k) \cdot \tilde{\mathbf{E}}(p)] \\ &\times \left[1 + \int_0^1 dx \int_0^{1-x} dy \frac{2m^2}{x(1-x)k^2 + y(1-y)p^2 + 2xy p \cdot k - m^2} \right], \end{aligned} \quad (\text{C1})$$

where p and k are the two photon momenta and are related to that of the axial current as $q^\mu = p^\mu + k^\mu$ according to the momentum conservation. The first and second terms in the brackets are the anomalous term and the matrix element of the pseudoscalar condensate, respectively. The tilde on the field strengths stands for the Fourier spectrum throughout the paper.

We show that the AWIs in Eqs. (19) and (C1) exactly agree with each other in a certain limit. This agreement occurs in the limit where one of the photon momentum is zero while the other is finite. We shall take $p^\mu \rightarrow 0$, and then $q^\mu = k^\mu$ led by the momentum conservation. Then, the AWI (C1) reads

$$\text{F.T. } \langle p, k | \partial_\mu j_A^\mu | 0 \rangle|_{p=0} = \frac{q_f^2}{2\pi^2} \cdot \frac{1}{2} [\tilde{\mathbf{E}}(q) \cdot \tilde{\mathbf{B}}(0) + \tilde{\mathbf{B}}(q) \cdot \tilde{\mathbf{E}}(0)] \left[1 - I\left(\frac{q^2}{4m^2}\right) \right]. \quad (\text{C2})$$

Remarkably, the integral in Eq. (C1) has reduced to the I function (9) involved in the LLL approximation. One can show this reduction as follows. We have

$$\int_0^1 dx \int_0^{1-x} dy \frac{2m^2}{x(1-x)k^2 - m^2} = \int_0^1 dx \frac{2m^2(1-x)}{x(1-x)k^2 - m^2}, \quad (\text{C3})$$

and notice the identical transformations

$$\begin{aligned} \int_0^1 dx \frac{2m^2(1-x)}{x(1-x)k^2 - m^2} &= \int_0^1 dx \frac{2m^2x}{(1-x)xk^2 - m^2} = \frac{1}{2} \int_0^1 dx \frac{2m^2}{x(1-x)k^2 - m^2} \\ &= -I(k^2/4m^2). \end{aligned} \quad (\text{C4})$$

The sum of the first two expressions results in the third expression that is nothing but the I function. When one sends the other momentum k^μ to zero and maintains a finite value of p^μ , the integral reduces to the I function in the same manner. We consider the case of $\tilde{\mathbf{E}}(0) = 0$. Summing the two contributions from $\tilde{\mathbf{B}}(p = 0)$ and $\tilde{\mathbf{B}}(k = 0)$ in Eq. (C1), we obtain

$$\text{F.T. } \langle q | \partial_\mu j_A^\mu | 0 \rangle = \frac{q_f^2}{2\pi^2} \tilde{\mathbf{E}}(q) \cdot \tilde{\mathbf{B}}(0) \left[1 - I\left(\frac{q^2}{4m^2}\right) \right]. \quad (\text{C5})$$

Therefore, the AWI (19) in the LLL agrees with Eq. (C5) when one further assumes a homogeneity, i.e., $|\mathbf{q}_\perp| = 0$, in the plane transverse to the magnetic field. In this limit, the Gaussian factor goes away in Eq. (19) and the squared momentum q^2 reduces to q_\parallel^2 .

Now, we show that the vanishing momentum limit corresponds to a constant electromagnetic field (though the gauge field itself depends on the spacetime coordinate). Remember that the LLL contribution is computed in the homogeneous limit. For simplicity, we may consider a parallel electromagnetic field in the third spatial direction. Such a parallel field can be described by a linear gauge configuration

$$A^\mu(x) = (-c_0 z E_0(\mathbf{x}_\perp), -d_1 y B_0(t, z), d_2 x B_0(t, z), -c_3 t E_0(\mathbf{x}_\perp)), \quad (\text{C6})$$

with constants such that $c_0 + c_3 = 1$ and $d_1 + d_2 = 1$. One can still let the fields have spacetime dependences within $E_0(\mathbf{x}_\perp)$ and $B_0(t, z)$. The gauge transformation does not change the following observations, because we examine the strengths of the electric and magnetic fields

$$\tilde{E}_z(p) = \tilde{E}_0(\mathbf{p}_\perp) [c_3 \omega \delta'(\omega) \delta(p_z) + c_0 p_z \delta'(p_z) \delta(\omega)] = (2\pi)^2 \delta(\omega) \delta(p_z) \tilde{E}_0(\mathbf{p}_\perp), \quad (\text{C7a})$$

$$\tilde{B}_z(p) = \tilde{B}_0(\omega, p_z) [d_2 p_x \delta'(p_x) \delta(p_y) + d_1 p_y \delta(p_x) \delta'(p_y)] = (2\pi)^2 \delta(p_x) \delta(p_y) \tilde{B}_0(\omega, p_z), \quad (\text{C7b})$$

where $\omega = p^0$. The prime on the delta function stands for the derivative with respect to the argument. One can read off the Fourier spectra. When the electric field is independent of t and z , its Fourier spectrum corresponds to vanishing ω and q_z in spite of the facts that q^μ is the momentum of the gauge field and the gauge field itself depends on t and z . In a similar manner, when the magnetic field is independent of x and y , its Fourier spectrum corresponds to vanishing q_x and q_y . When the electromagnetic field is independent of all the spacetime coordinates, one gets the four-dimensional delta functions

$$\tilde{E}_z(p) = (2\pi)^4 \delta^{(4)}(p) E, \quad (\text{C8a})$$

$$\tilde{B}_z(p) = (2\pi)^4 \delta^{(4)}(p) B, \quad (\text{C8b})$$

with E and B being constant strengths. Therefore, the AWIs in Eqs. (19) and (C1) exactly agree with one another in the limits of constant magnetic field and of the homogeneous electric field over the extension of cyclotron orbits. As already discussed in Sec. IV B 1, the absence of the Gaussian factor can be understood intuitively.

It is interesting to extend the above relation to finite temperature and/or density. The AWI in the LLL approximation is already given in Eq. (18). The massive triangle diagrams may be straightforwardly extended to finite temperature and/or density as well. We leave explicit computations as an open issue.

-
- [1] Koichi Hattori and Kazunori Itakura, “In-medium polarization tensor in strong magnetic fields (I): Magneto-birefringence at finite temperature and density,” (2022), [arXiv:2205.04312 \[hep-ph\]](#).
 - [2] Dmitri E. Kharzeev, Larry D. McLerran, and Harmen J. Warringa, “The Effects of topological charge change in heavy ion collisions: ‘Event by event P and CP violation’,” [Nucl.Phys. **A803**, 227–253 \(2008\)](#), [arXiv:0711.0950 \[hep-ph\]](#).
 - [3] Kenji Fukushima, Dmitri E. Kharzeev, and Harmen J. Warringa, “The Chiral Magnetic Effect,” [Phys. Rev. **D78**, 074033 \(2008\)](#), [arXiv:0808.3382 \[hep-ph\]](#).
 - [4] D. E. Kharzeev, J. Liao, S. A. Voloshin, and G. Wang, “Chiral magnetic and vortical effects in high-energy nuclear collisions—status report,” [Prog. Part. Nucl. Phys. **88**, 1–28 \(2016\)](#), [arXiv:1511.04050 \[hep-ph\]](#).
 - [5] Vladimir Skokov, Paul Sorensen, Volker Koch, Soeren Schlichting, Jim Thomas, Sergei Voloshin, Gang Wang, and Ho-Ung Yee, “Chiral Magnetic Effect Task Force Report,” [Chin. Phys. **C41**, 072001 \(2017\)](#), [arXiv:1608.00982 \[nucl-th\]](#).
 - [6] Koichi Hattori and Xu-Guang Huang, “Novel quantum phenomena induced by strong magnetic fields in heavy-ion collisions,” [Nucl. Sci. Tech. **28**, 26 \(2017\)](#), [arXiv:1609.00747 \[nucl-th\]](#).
 - [7] A. A. Burkov, “Chiral anomaly and transport in Weyl metals,” [J. Phys. Condens. Matter **27**, 113201 \(2015\)](#), [arXiv:1502.07609 \[cond-mat.mes-hall\]](#).
 - [8] E. V. Gorbar, V. A. Miransky, I. A. Shovkovy, and P. O. Sukhachov, “Anomalous transport properties of Dirac and Weyl semimetals (Review Article),” [Low Temp. Phys. **44**, 487–505 \(2018\)](#), [arXiv:1712.08947 \[cond-mat.mes-hall\]](#).

- [9] N. P. Armitage, E. J. Mele, and Ashvin Vishwanath, “Weyl and Dirac semimetals in three-dimensional solids,” [Reviews of Modern Physics](#) **90**, 015001 (2018), [arXiv:1705.01111 \[cond-mat.str-el\]](#).
- [10] Yukinao Akamatsu and Naoki Yamamoto, “Chiral Plasma Instabilities,” [Phys. Rev. Lett.](#) **111**, 052002 (2013), [arXiv:1302.2125 \[nucl-th\]](#).
- [11] Naoki Yamamoto, “Chiral transport of neutrinos in supernovae: Neutrino-induced fluid helicity and helical plasma instability,” [Phys. Rev. D](#) **93**, 065017 (2016), [arXiv:1511.00933 \[astro-ph.HE\]](#).
- [12] Naoki Yamamoto and Di-Lun Yang, “Chiral Radiation Transport Theory of Neutrinos,” [Astrophys. J.](#) **895**, 56 (2020), [arXiv:2002.11348 \[astro-ph.HE\]](#).
- [13] Michael S. Turner and Lawrence M. Widrow, “Inflation Produced, Large Scale Magnetic Fields,” [Phys. Rev.](#) **D37**, 2743 (1988).
- [14] Sean M. Carroll, George B. Field, and Roman Jackiw, “Limits on a Lorentz and Parity Violating Modification of Electrodynamics,” [Phys. Rev.](#) **D41**, 1231 (1990).
- [15] W. Daniel Garretson, George B. Field, and Sean M. Carroll, “Primordial magnetic fields from pseudoGoldstone bosons,” [Phys. Rev.](#) **D46**, 5346–5351 (1992), [arXiv:hep-ph/9209238 \[hep-ph\]](#).
- [16] M. Joyce and Mikhail E. Shaposhnikov, “Primordial magnetic fields, right-handed electrons, and the Abelian anomaly,” [Phys. Rev. Lett.](#) **79**, 1193–1196 (1997), [arXiv:astro-ph/9703005 \[astro-ph\]](#).
- [17] Massimo Giovannini, “The Magnetized universe,” [Int. J. Mod. Phys. D](#) **13**, 391–502 (2004), [arXiv:astro-ph/0312614](#).
- [18] M. Laine, “Real-time Chern-Simons term for hypermagnetic fields,” [JHEP](#) **10**, 056 (2005), [arXiv:hep-ph/0508195](#).
- [19] Mohamed Abdallah *et al.* (STAR), “Search for the chiral magnetic effect with isobar collisions at $\sqrt{s_{NN}}=200$ GeV by the STAR Collaboration at the BNL Relativistic Heavy Ion Collider,” [Phys. Rev. C](#) **105**, 014901 (2022), [arXiv:2109.00131 \[nucl-ex\]](#).
- [20] Naoto Tanji, Niklas Mueller, and Jurgen Berges, “Transient anomalous charge production in strong-field QCD,” [Phys. Rev.](#) **D93**, 074507 (2016), [arXiv:1603.03331 \[hep-ph\]](#).
- [21] Niklas Mueller, Soren Schlichting, and Sayantan Sharma, “Chiral magnetic effect and anomalous transport from real-time lattice simulations,” [Phys. Rev. Lett.](#) **117**, 142301 (2016),

- [arXiv:1606.00342 \[hep-ph\]](#).
- [22] De-fu Hou and Shu Lin, “Fluctuation and Dissipation of Axial Charge from Massive Quarks,” *Phys. Rev. D* **D98**, 054014 (2018), [arXiv:1712.08429 \[hep-ph\]](#).
 - [23] Naoto Tanji, “Nonequilibrium axial charge production in expanding glasma flux tubes,” *Phys. Rev. D* **D98**, 014025 (2018), [arXiv:1805.00775 \[hep-ph\]](#).
 - [24] Patrick Copinger, Kenji Fukushima, and Shi Pu, “Axial Ward identity and the Schwinger mechanism – Applications to the real-time chiral magnetic effect and condensates,” *Phys. Rev. Lett.* **121**, 261602 (2018), [arXiv:1807.04416 \[hep-th\]](#).
 - [25] Hidetoshi Taya, “Dynamically assisted Schwinger mechanism and chirality production in parallel electromagnetic field,” *Phys. Rev. Res.* **2**, 023257 (2020), [arXiv:2003.08948 \[hep-ph\]](#).
 - [26] Berndt Müller and Di-Lun Yang, “Anomalous spin polarization from turbulent color fields,” *Phys. Rev. D* **105**, L011901 (2022), [arXiv:2110.15630 \[nucl-th\]](#).
 - [27] Di-Lun Yang, “Quantum kinetic theory for spin transport of quarks with background chromo-electromagnetic fields,” (2021), [arXiv:2112.14392 \[hep-ph\]](#).
 - [28] Dorota Grabowska, David B. Kaplan, and Sanjay Reddy, “Role of the electron mass in damping chiral plasma instability in Supernovae and neutron stars,” *Phys. Rev. D* **D91**, 085035 (2015), [arXiv:1409.3602 \[hep-ph\]](#).
 - [29] E. V. Gorbar and I. A. Shovkovy, “Chiral anomalous processes in magnetospheres of pulsars and black holes,” (2021), [arXiv:2110.11380 \[astro-ph.HE\]](#).
 - [30] Valerie Domcke, Yohei Ema, and Kyohei Mukaida, “Chiral Anomaly, Schwinger Effect, Euler-Heisenberg Lagrangian, and application to axion inflation,” *JHEP* **02**, 055 (2020), [arXiv:1910.01205 \[hep-ph\]](#).
 - [31] A. Boyarsky, V. Cheianov, O. Ruchayskiy, and O. Sobol, “Evolution of the Primordial Axial Charge across Cosmic Times,” *Phys. Rev. Lett.* **126**, 021801 (2021), [arXiv:2007.13691 \[hep-ph\]](#).
 - [32] Stephen L. Adler, “Axial vector vertex in spinor electrodynamics,” *Phys. Rev.* **177**, 2426–2438 (1969).
 - [33] J. S. Bell and R. Jackiw, “A PCAC puzzle: $\pi^0 \rightarrow \gamma\gamma$ in the sigma model,” *Nuovo Cim.* **A60**, 47–61 (1969).
 - [34] Stephen L. Adler and William A. Bardeen, “Absence of higher order corrections in the anomalous axial vector divergence equation,” *Phys. Rev.* **182**, 1517–1536 (1969).

- [35] Hiroshi Itoyama and Alfred H. Mueller, “The Axial Anomaly at Finite Temperature,” [Nucl. Phys. B](#) **218**, 349–365 (1983).
- [36] Holger Bech Nielsen and Masao Ninomiya, “The Adler-Bell-Jackiw anomaly and Weyl fermions in a crystal,” [Phys. Lett.](#) **130B**, 389–396 (1983).
- [37] Jan Ambjorn, J. Greensite, and C. Peterson, “The Axial Anomaly and the Lattice Dirac Sea,” [Nucl. Phys.](#) **B221**, 381–408 (1983).
- [38] Michael Creutz, “Aspects of Chiral Symmetry and the Lattice,” [Rev. Mod. Phys.](#) **73**, 119–150 (2001), [arXiv:hep-lat/0007032 \[hep-lat\]](#).
- [39] Michael E. Peskin and Daniel V. Schroeder, [An Introduction to quantum field theory](#) (1995).
- [40] Koichi Hattori and Kazunori Itakura, “Vacuum birefringence in strong magnetic fields: (I) Photon polarization tensor with all the Landau levels,” [Annals Phys.](#) **330**, 23–54 (2013), [arXiv:1209.2663 \[hep-ph\]](#).
- [41] Koichi Hattori and Daisuke Satow, “Gluon Spectrum in Quark-Gluon Plasma under Strong Magnetic Fields,” [Phys. Rev.](#) **D97**, 014023 (2018), [arXiv:1704.03191 \[hep-ph\]](#).
- [42] Julian S. Schwinger, “Gauge Invariance and Mass,” [Phys. Rev.](#) **125**, 397–398 (1962).
- [43] Julian S. Schwinger, “Gauge Invariance and Mass. 2.” [Phys. Rev.](#) **128**, 2425–2429 (1962).
- [44] Kenji Fukushima, Koichi Hattori, Ho-Ung Yee, and Yi Yin, “Heavy Quark Diffusion in Strong Magnetic Fields at Weak Coupling and Implications for Elliptic Flow,” [Phys. Rev.](#) **D93**, 074028 (2016), [arXiv:1512.03689 \[hep-ph\]](#).
- [45] Andrei V. Smilga, “Anomaly mechanism at finite temperature,” [Phys. Rev.](#) **D45**, 1378–1394 (1992).
- [46] J. F. Donoghue, E. Golowich, and Barry R. Holstein, “Dynamics of the standard model,” [Camb. Monogr. Part. Phys. Nucl. Phys. Cosmol.](#) **2**, 1–540 (1992), [Camb. Monogr. Part. Phys. Nucl. Phys. Cosmol.35(2014)].
- [47] P.A. Zyla *et al.* (Particle Data Group), “Review of Particle Physics,” [PTEP](#) **2020**, 083C01 (2020).
- [48] George Gamow, *One, two, three–infinity: facts and speculations of science* (Courier Corporation, 1988).
- [49] Yukinao Akamatsu and Naoki Yamamoto, “Chiral Langevin theory for non-Abelian plasmas,” [Phys. Rev.](#) **D90**, 125031 (2014), [arXiv:1402.4174 \[hep-th\]](#).
- [50] Jianhui Zhou, Hao-Ran Chang, and Di Xiao, “Plasmon mode as a detection of the chiral

- anomaly in weyl semimetals,” [Phys. Rev. B **91**, 035114 \(2015\)](#).
- [51] Jan Behrends, Adolfo G. Grushin, Teemu Ojanen, and Jens H. Bardarson, “Visualizing the chiral anomaly in dirac and weyl semimetals with photoemission spectroscopy,” [Phys. Rev. B **93**, 075114 \(2016\)](#).
 - [52] C. J. Tabert, J. P. Carbotte, and E. J. Nicol, “Optical and transport properties in three-dimensional dirac and weyl semimetals,” [Phys. Rev. B **93**, 085426 \(2016\)](#).
 - [53] Jinho Yang, Jeehoon Kim, and Ki-Seok Kim, “Transmission and reflection coefficients and faraday/kerr rotations as a function of applied magnetic fields in spin-orbit coupled dirac metals,” [Phys. Rev. B **98**, 075203 \(2018\)](#).
 - [54] Kabyashree Sonowal, Ashutosh Singh, and Amit Agarwal, “Giant optical activity and kerr effect in type-i and type-ii weyl semimetals,” [Phys. Rev. B **100**, 085436 \(2019\)](#).
 - [55] Zhida Song, Jimin Zhao, Zhong Fang, and Xi Dai, “Detecting the chiral magnetic effect by lattice dynamics in weyl semimetals,” *Physical Review B* **94**, 214306 (2016).
 - [56] Pierre Rinkel, Pedro LS Lopes, and Ion Garate, “Signatures of the chiral anomaly in phonon dynamics,” *Physical review letters* **119**, 107401 (2017).
 - [57] Aaron Hui, Yi Zhang, and Eun-Ah Kim, “Optical signatures of the chiral anomaly in mirror-symmetric weyl semimetals,” *Physical Review B* **100**, 085144 (2019).
 - [58] Xiang Yuan, Cheng Zhang, Yi Zhang, Zhongbo Yan, Tairu Lyu, Mengyao Zhang, Zhilin Li, Chaoyu Song, Minhao Zhao, Pengliang Leng, *et al.*, “The discovery of dynamic chiral anomaly in a weyl semimetal nbas,” *Nature communications* **11**, 1–7 (2020).
 - [59] Sultan Almutairi, Qianfan Chen, Mikhail Tokman, and Alexey Belyanin, “Four-wave mixing in Weyl semimetals,” [Phys. Rev. B **101**, 235156 \(2020\)](#).
 - [60] Yang Gao and Furu Zhang, “Current-induced second harmonic generation of dirac or weyl semimetals in a strong magnetic field,” [Phys. Rev. B **103**, L041301 \(2021\)](#).
 - [61] Ashutosh Singh and J. P. Carbotte, “Temperature effects in tilted weyl semimetals: Dichroism and dynamic hall angle,” [Phys. Rev. B **103**, 075114 \(2021\)](#).
 - [62] Zhongqu Long, Yongrui Wang, Maria Erukhimova, Mikhail Tokman, and Alexey Belyanin, “Magnetopolaritons in weyl semimetals in a strong magnetic field,” [Phys. Rev. Lett. **120**, 037403 \(2018\)](#).
 - [63] Wang-Kong Tse and A. H. MacDonald, “Giant magneto-optical kerr effect and universal faraday effect in thin-film topological insulators,” [Phys. Rev. Lett. **105**, 057401 \(2010\)](#).

- [64] Long Liang, P. O. Sukhachov, and A. V. Balatsky, “Axial magnetoelectric effect in dirac semimetals,” [Phys. Rev. Lett. **126**, 247202 \(2021\)](#).
- [65] Mehdi Kargarian, Mohit Randeria, and Nandini Trivedi, “Theory of Kerr and Faraday rotations and linear dichroism in topological Weyl semimetals,” *Scientific reports* **5**, 1–10 (2015).
- [66] ID Tokman, Qianfan Chen, IA Shereshevsky, VI Pozdnyakova, Ivan Oladyshkin, Mikhail Tokman, and Alexey Belyanin, “Inverse faraday effect in graphene and weyl semimetals,” *Physical Review B* **101**, 174429 (2020).
- [67] P. Sikivie, “Experimental Tests of the Invisible Axion,” [Phys. Rev. Lett. **51**, 1415–1417 \(1983\)](#), [Erratum: *Phys.Rev.Lett.* 52, 695 (1984)].
- [68] Pierre Sikivie, “Detection Rates for ‘Invisible’ Axion Searches,” [Phys. Rev. D **32**, 2988 \(1985\)](#), [Erratum: *Phys.Rev.D* 36, 974 (1987)].
- [69] Georg G. Raffelt, “ASTROPHYSICAL AXION BOUNDS DIMINISHED BY SCREENING EFFECTS,” [Phys. Rev. D **33**, 897 \(1986\)](#).
- [70] Georg Raffelt and Leo Stodolsky, “Mixing of the Photon with Low Mass Particles,” [Phys. Rev. D **37**, 1237 \(1988\)](#).
- [71] Georg G. Raffelt, “Astrophysical methods to constrain axions and other novel particle phenomena,” [Phys. Rept. **198**, 1–113 \(1990\)](#).
- [72] Holger Gies, “Strong laser fields as a probe for fundamental physics,” [Eur. Phys. J. D **55**, 311–317 \(2009\)](#), [arXiv:0812.0668 \[hep-ph\]](#).
- [73] Javier Redondo and Andreas Ringwald, “Light shining through walls,” [Contemp. Phys. **52**, 211–236 \(2011\)](#), [arXiv:1011.3741 \[hep-ph\]](#).